RSC Advances

PAPER

View Article Online
View Journal | View Issue

Cite this: *RSC Adv.*, 2019, **9**, 24527

Novel porous organocatalysts for cycloaddition of CO_2 and epoxides†

Joel M. Kolle and Abdelhamid Sayari *

Received 16th July 2019
Accepted 31st July 2019

DOI: 10.1039/c9ra05466a

rsc.li/rsc-advances

Three classes of organosilicas (DMO, OMOs and PMOs) containing immobilized multi-hydroxyl bis-(quaternary ammonium) iodide salts were prepared and tested in the cycloaddition of CO_2 and epoxides. Owing to its higher surface area, pore volume and optimum nucleophilicity of the iodide ion, OMO-2 with two hydroxyl groups was found to be the most active catalyst. For substrates that are easy to activate such as propylene oxide, 1,2-epoxybutane and epichlorohydrin, excellent yields and selectivities were obtained under mild reaction conditions (0.5 MPa CO_2, 50 °C and 10–15 h). Moreover, OMO-2 showed very good catalytic properties (yield ≥ 93% and selectivity ≥ 98%), and excellent chemical and textural stability in the synthesis of 1,2-butylene carbonate over 5 cycles.

Introduction

Among greenhouse gases (GHGs), carbon dioxide (CO_2) is the main anthropogenic contributor to global warming and climate change.[1,2] Carbon capture is recognized as one of the most promising strategies to mitigate the adverse effects of CO_2 emissions.[3,4] Previously viewed largely as an industrial waste product, CO_2 is increasingly being valued as a cheap, readily available and non-toxic C1 source for the synthesis of chemicals and fuels.[5,6] Accordingly, CO_2 utilization is gaining popularity as a complementing tool to CO_2 capture and sequestration towards GHG mitigation. However, the inherent thermodynamic stability of CO_2 leads to low reactivity. As such, high CO_2 pressure and reaction temperature are generally required for its transformation. Nonetheless, combining CO_2 with highly reactive substrates such as epoxides and aziridines, in the presence of suitable catalysts, provides a pathway to overcome this energy barrier. The catalytic conversion of CO_2 and epoxides to cyclic carbonates (CCs) is one of many reactions using CO_2 as an alternative C1 feedstock. Application of CCs as aprotic polar solvents, active pharmaceutical ingredients, and monomers in the production of fine chemicals makes them an important group of organic materials in the chemical industry. In the generalized mechanism for the synthesis of CCs, regioselective CO_2 insertion is achieved by a combination of epoxide activation by Y through oxygen atom coordination and ring-opening by a nucleophile, X^- (Scheme 1).

A variety of homogeneous catalysts such as ionic liquids[7] and metal complexes;[8] immobilized catalysts including supported ionic liquids,[7] and traditional heterogeneous catalysts[9] were reported to be active towards CO_2 cycloaddition. On their own, the last group of catalysts showed low reactivity, and as such received less attention compared to free and immobilized homogeneous catalysts. The latter may consist of a single catalytic component, or a combination of a catalyst and a co-catalyst.[8] Examples of one-component catalyst include tributylpropylammonium iodide immobilized on silica,[10] quaternary ammonium[11] and phosphonium[12] salts. Two-component catalysts include benzylbromide/DMF,[13] tetrabutylammonium salt/EDTA,[14] and polymer-supported quaternary onium salts/aqueous solutions of metal salts.[15] These catalysts are not highly popular as they increase the complexity of the process, leading to tedious catalyst separation/recovery and product purification steps. Accordingly, to achieve simplified and cost-effective chemical processes, one-component catalysts are preferred.

One-component catalysts can be mono- or bifunctional in nature. Mono-functional catalysts such as alkyl quaternary ammonium[16] or phosphonium[17] halides play a single role, which consists of opening the epoxide ring, leading to the insertion of CO_2. These extensively investigated catalysts were found to exhibit good to excellent yields in the cycloaddition of CO_2 and epoxides.[18,19] Moreover, one-component bifuntional homogeneous or immobilized catalysts may contain specific functional groups, such as –COOH, $–NH_2$ and –OH or metals

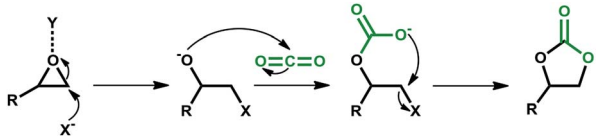

Scheme 1 Synthesis of cyclic carbonate from epoxide and CO_2.

Centre for Catalysis Research and Innovation (CCRI), Department of Chemistry, University of Ottawa, Ottawa, Ontario, Canada K1N 6N5. E-mail: Abdel.Sayari@uottawa.ca

† Electronic supplementary information (ESI) available. See DOI: 10.1039/c9ra05466a

(*e.g.* Zn, Co and Al). Bifunctionality implies that the catalytic material plays two roles in the course of the reaction, namely; (1) activation of the epoxide by the functional groups,[20] rendering it more susceptible to undergo cycloaddition – Y in Scheme 1, and (2) opening of the epoxide ring by the halide ion,[21] similar to the mono-functional catalysts, X^- in Scheme 1. The above functional groups activate the epoxides *via* hydrogen bonding, while epoxide activation by metal occurs through the formation of metalalkoxides *via* Lewis acid interactions.[22,23] Examples of metal-free one-component bifunctional catalysts include free and supported hydroxylalkyl ammonium salts[11] or phosphonium[17] salts. Regardless of the design, type or functionality of the catalyst, the ring opening of all epoxides requires a nucleophile. The iodide ion was reported as one of the most efficient owing to its exceptional leaving group ability, stemming from its bulky nature and lower electronegativity.

In terms of sustainable and low-cost processes, highly active metal-free one-component bifunctional catalysts with stable active sites and easy reusability are attractive. Many such catalysts, covalently anchored onto a variety of solid materials were reported in the literature.[24] In some cases, these hybrid solids demonstrate similar or even better activities compared to their homogeneous counterparts.[17,25] Porous inorganic solids such as mesoporous SBA-15 silica[26,27] was used as support for one-component porous hybrid solid (PHS) catalysts for the synthesis of cyclic carbonates. Compared to organic supports such as polystyrene, they offer better thermal and mechanical stability, enhanced chemical interaction between the support and the active organic species and high loading of active sites, thereby enhancing production. Moreover, mesoporous inorganic supports alleviate molecular traffic within the pore system, which could enhance both the rate and selectivity of the reaction.

The main preparation method for PHS entails post-synthesis surface functionalization of a silica; typically through grafting of an aminosilane or phosphine–silane, followed by quaternization to afford an immobilized quaternary ammonium or phosphonium salt – Scheme 2a. Often, such organosilicas consist of a disordered distribution of the organic moieties; hence these solids may be referred to as disordered mesoporous organosilicas (DMO). Alternatively, the co-condensation of a silica network former (*e.g.* TEOS or TMOS) and an organosilica precursor (organotrialkoxysilanes, bridged- or poly-silsesquioxanes) over a structure directing agent is a one-pot synthesis method to obtain ordered mesoporous organosilicas (OMOs) – Scheme 2b. Furthermore, a distinctive group of mesoporous organocatalysts, with a unique homogeneous distribution and high loading of covalently linked organic functionalities within the silica framework are periodic mesoporous organosilicas (PMOs). These materials are derived from the hydrolytic sol–gel polycondensation of organic bridged-silsesquioxanes ($R[Si(OR')_3]_n$; $n \geq 2$) in the presence of surfactant templates without addition of silica precursors – Scheme 2c.

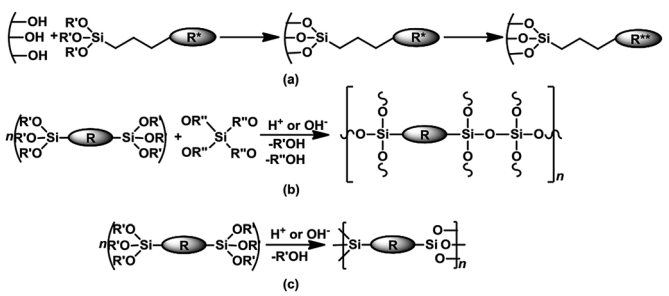

Scheme 2 Synthesis of (a) DMO *via* surface grafting and quaternization (b) OMO *via* the co-condensation route (c) periodic mesoporous organosilicas – PMO.

Significant progress in the synthesis of CCs from CO_2 and epoxides over mesoporous organocatalysts derived by the grafting of aminosilane followed by quaternization (Scheme 2a) has been reported in a number of reviews.[7,28] Although OMOs containing ammonium halides,[29,30] and PMOs containing melamine[31] and urea[32] moieties were reported as active catalysts in the synthesis of CCs, OMOs and PMOs received noticeably less attention compared to DMOs. Considering the higher surface area of OMOs compared to DMOs, and the significantly higher organic content achievable with PMOs, organocatalysts with greater surface area and active sites can be obtained from OMOs and PMOs respectively. If such active sites can be readily accessed, a significant enhancement in catalytic performance (*i.e.* higher reaction rates, selectivity and yield) can be expected. In addition, higher active site density is expected to enhance catalytic activity. In this sense, homogeneous[33] and heterogeneous[34] organocatalysts containing two active sites per molecule were found to be more effective than those containing only one. In this contribution, we present four groups of novel immobilized multi-hydroxyl bis-(quaternary ammonium) salts prepared *via* three routes: (1) grafting of a bridged-SQ on silicas, followed by quaternization, (2) co-condensation of (i) bridged-SQ and (ii) poly-SQ with TEOS, and (3) PMOs derived from (i) bridge-SQ and (ii) poly-SQ. Furthermore, their activity in the synthesis of CCs from CO_2 and epoxides under mild reaction conditions was discussed. The reusability of the most active catalyst was also investigated to better understand the catalyst performance (yield and selectivity), chemical stability (resistance to leaching) and structural stability (textural properties) with reuse.

Experimental

Materials

N,*N*′-Bis(2-hydroxyethyl)-*N*,*N*′-bis(trimethoxysilylpropyl)ethylenediamine – BHBPD (66–68% in methanol) was purchased from Gelest. Chromatography grade silica gel mesh 230–400 (hereafter referred to as SiL), 2-iodoethanol (99%), ammonium iodide (99.5%), P123 (average $M_n \sim 5800$), tetraethyl orthosilicate – TEOS (98%), 3-chloropropyltrimethoxysilane – 3CPTS (97%), styrene oxide (97%), propylene oxide – PO (99%), 1,2-epoxybutane – 1,2-EB (99%), epichlorohydrin (99%), cyclohexene oxide – CHO (98%), 3-glycidoxypropyltrimethoxysilane (GPS), triethylamine – TEA (99%) and KCl (99%) were purchased from Sigma Aldrich. Ethyl acetate (99.9%), diethyl ether – Et_2O (99.8%), ethanol (99%), methanol (99%), hydrochloric acid

(37%) and toluene (99%) were obtained from Fischer. P-10 and Q-10 mesoporous silica supports were donated by Fuji Silysia Chemical Ltd. Chloroform-D was obtained from Cambridge Isotope Laboratories. All chemicals were used as obtained with no further purification. Carbon dioxide (99.998%) was obtained from Linde AG.

Preparation of mesoporous organosilica materials

Method A: preparation of DMOs *via* grafting and quaternization of amine. Three commercial grade silicas (Q-10, P-10 and SiL) and SBA-15 silica were used as supports. SBA-15 was prepared using an established procedure.[35] Grafting was carried out in toluene in the presence of water. Our group previously demonstrated that addition of water improves both the quality and loading of grafted amine on MCM-41.[36] Based on literature reports,[37] it is possible to estimate the amount of water required to obtain a fully hydroxylated silica surface. This can be achieve by considering the maximum number of surface silanol groups to be 5×10^{18} SiOH per m^2, and by introducing twice as many water molecules per m^2.[38] Accordingly, for a typical silica with a surface area of 300 $m^2\ g^{-1}$, the volume of water to be added is approximately 0.1 mL g^{-1}.

A typical procedure for grafting was as follows; 1 g of thermally pretreated (at 130 °C for 4 h) silica was dispersed in 30 mL of toluene at room temperature, followed by addition of an appropriate volume of water; 0.1 mL for Q-10 and P-10, 0.15 mL for SiL, and 0.3 mL for SBA-15. The temperature of the mixture was raised to 85 °C and further stirred for 30 min. Finally, 2 mL of BHBPD was added and the resultant mixture was refluxed at 85 °C for 16 h in an oil bath. The grafted materials were then filtered, washed with toluene, methanol, then Et_2O, and dried under vacuum at 60 °C for 4 h. The obtained solids are hereafter referred to as S@amine, where S indicates the support. The amine-grafted solids were then quaternized as follows: 1 g of material was dispersed in 15 mL of toluene, followed by addition of 2 mL of 2-iodoethanol under a nitrogen atmosphere. The reaction mixture was kept under reflux at 70 °C for 3 days. The obtained solids were filtered off, washed with toluene, methanol, then Et_2O, and dried at 70 °C under vacuum for 4 h to yield pale yellow powder materials of immobilized diammonium iodide salt. The obtained solids are hereafter referred to as DMO-Q10, DMO-P10, DMO-SiL and DMO-SBA15 after the corresponding S@amine. The synthesis of amine-grafted materials and their quaternized counterparts is represented in Scheme 3, with Q-10 as silica support.

Method B: preparation of OMOs *via* co-condensation of BHBPD or poly-SQ salt and TEOS. The synthesis of all porous organosilica by hydrolysis and condensation with a silica precursor were performed in the presence of a neutral surfactant (P123) under acidic condition. In a typical procedure, 2.0 g of triblock copolymer P123 and 2 g of KCl were dissolved in a mixture of 30 g distilled water and 60 g of 2 M HCl solution in a 250 mL Teflon-liner at 40 °C. Notice that the use of KCl was shown to enhance ordering of mesoporous organosilicas.[39] To this solution, 4.3 g of TEOS was added and the mixture stirred for 1 h to ensure the pre-hydrolysis of TEOS. Thereafter, 2 mL (2.83 mmol) of BHBPD, corresponding to a nominal amine loading of 2.0 mmol per gram of silica, was slowly added under stirring. The resultant mixture was further stirred at 40 °C for 20 h. Finally, the mixture was transferred into an autoclave and heated at 100 °C under static condition for 2 days. The solid products were collected by filtration, washed with water, and dried at ambient conditions. The surfactant was removed by refluxing in 100 mL of a 98 : 2 v/v% ratio of ethanol : conc. HCl mixture at 60 °C for 6 h. The powder material was collected by filtration, washed with ethanol, and dried at ambient conditions. A similar preparation, but without BHBPD, was carried out for SBA-15 silica, herein referred to as SBA-15*. To make sure all P123 has been removed, 1 g of the solid ethanol-extracted material was subjected to additional Soxhlet extraction with 100 mL of methanol at 70 °C for 16 h. The obtained solid was dried overnight in ambient condition, then at 60 °C under vacuum for 4 h.

An off-white powder material, hereafter referred to as OMO-1, was obtained from the co-condensation of TEOS and BHBPD. Because of the acidic conditions, OMO-1 was actually in the form of a quaternary ammonium chloride salt. OMO-1 was subjected to; (1) ion-exchange with ammonium iodide to obtain the corresponding ammonium iodide salt – OMO-2 and (2) dequaternization, regenerate the amine – OMO-3. To obtain a QAS with additional –OH groups, OMO-3 was quaternized with 2-iodoethanol to afford OMO-4. The structures of OMO-(1–4) are represented in Scheme 4.

Ion-exchange was carried out as follows; 1 g of OMO-1 was dissolved in 30 mL of methanol followed by addition of 1 mL of ammonium iodide under a nitrogen atmosphere. The mixture was refluxed at 65 °C for 16 h. The resultant solid was recovered by filtration, washed with methanol, then Et_2O and dried under vacuum at 70 °C for 4 h to afford a yellow powder (OMO-2). To regenerate the amine from OMO-1, 1 g of material was dispersed in 50 mL of ethanol, followed by the addition of 1 mL

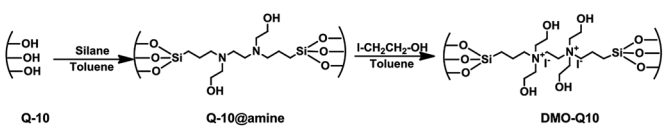

Scheme 3 Synthesis of Q-10@amine and DMO-Q10 *via* grafting and quaternization.

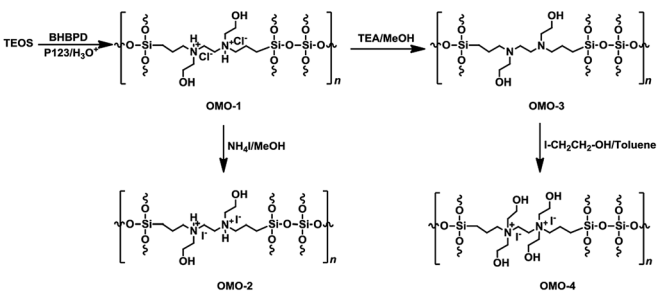

Scheme 4 Synthesis of OMO-1 to OMO-4 *via* co-condensation followed by ion-exchange or quaternization.

of triethylamine. After reflux at 60 °C for 2 h, the solid was recovered by hot-filtration and washed with boiling ethanol, then dried at 60 °C under vacuum for 4 h to afford an off-white powder material – OMO-3. OMO-3 was quaternized as described in method A to afford a yellow powder – OMO-4.

The preparation of OMOs from BHBPD-derived salt involves two steps; the synthesis of the salt, hereafter referred to as poly-SQ salt, followed by its co-condensation with TEOS. The poly-SQ salt was synthesized as follows; to a 25 mL two-neck round bottom flask containing 10 mL of toluene, 2 mL (2.83 mmol) of BHBPD was added. Under a nitrogen atmosphere, 2.0 equivalent of 3-chloropropyltrimethoxysilane was added. The reaction flask was sealed under nitrogen and refluxed at 85 °C for 24 h. Toluene and unreacted reagents were removed under reduced pressure at 90 °C to afford a brownish-yellow liquid. The procedure for the co-condensation of the poly-SQ salt and TEOS was similar to that of BHBPD and TEOS (OMO-1). An amount of poly-SQ salt was added to a pre-hydrolyzed TEOS solution with a nominal amine loading of 2.0 mmol per gram of silica. The template was extracted as described for OMO-1 to afford a light grey solid denoted OMO-5. Ion-exchange of OMO-5 with ammonium iodide (as described for OMO-1) produced a yellow solid, OMO-6 (Scheme 5).

Method C: synthesis of PMOs *via* condensation of BHBPD and poly-SQ salt. To an aqueous solution of P123, prepared as described in method B, 2 mL of BHBPD or 2.8 mL of poly-SQ salt was added slowly under stirring. The resultant mixture was further stirred at 40 °C for 20 h, and the mixture was transferred into an autoclave and heated at 100 °C under static condition for 2 days. The solid products were collected by filtration, washed with water, and dried at ambient conditions. Surfactant extraction, ion-exchange, dequaternization and quaternization were carried out on the resultant solid as described for OMO-1. All PMOs are represented in Scheme 6. PMO-1 and PMO-3 were obtained as off-white solids; PMO-5 was light-grey; and PMO-2, PMO-4 and PMO-6 were yellow powder materials.

Characterization of materials

Textural properties and organic content. The specific surface area, pore volume and mean pore diameter of all materials were determined by nitrogen adsorption–desorption measurements at −196 °C on a Micromeritics 2020 instrument, as reported earlier.[10] Samples were degassed under nitrogen for 4 h at 120 °C prior to analysis. Specific surface areas were calculated using the BET method at relative pressures of 0.06 to 0.2. The total pore volume (V_p) was recorded at $p/p_0 = 0.99$ to exclude possible interparticle pores. The average pore size (D_p) was determined using the density functional theory.

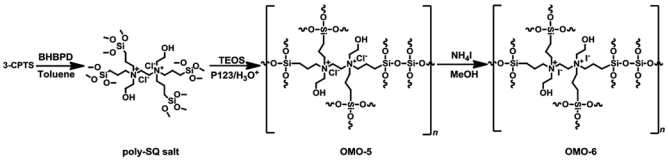

Scheme 5 Synthesis of poly-SQ salt and OMO-5 and OMO-6 *via* co-condensation followed by ion-exchange.

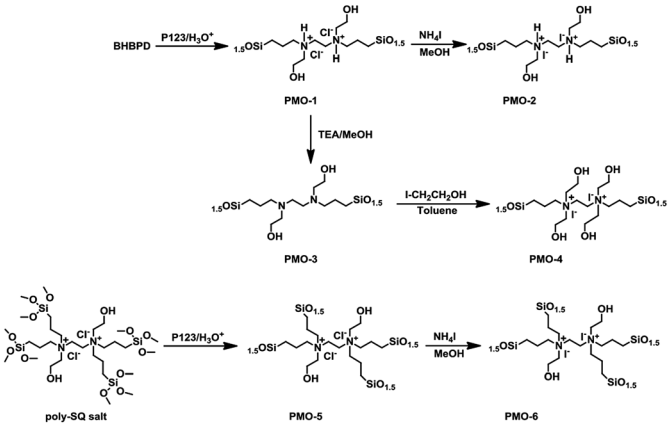

Scheme 6 Synthesis of PMOs *via* condensation of (top) BHBPD, and (bottom) poly-SQ salt.

The organic or nitrogen content (N-content) of all organosilicas was determined using thermogravimetric analysis (TGA) on a TA Q500 instrument. Sample were heated to 120 °C at 10 °C min^{-1} under flowing nitrogen and held for 30 min, to ensure the removal of physisorbed species (*e.g.* water and solvents). Then the temperature was raised to 800 °C under flowing nitrogen, then air at 800 °C for 10 min. The organic content was calculated based on the weight loss beyond 200 °C.

IR spectroscopy. To identity the incorporated organic species, ATR-IR measurements were recorded on a Nicolet 6700 spectrometer equipped with a liquid N_2-cooled MTC-A (mercury–tellurium–cadmium) detector and a Fisher Scientific horizontal ATR unit with a ZnSe crystal. For this, a few mg of powder sample was homogeneously spread onto the surface of the ATR crystal, and the IR spectra were recorded from 600 to 4000 cm^{-1} at a resolution of 2 cm^{-1} using 128 scans. For each scanning, the spectrum was collected by subtracting air (background) spectrum from the original spectrum. All ATR-FTIR experiments were run in triplicate to ensure the reproducibility of the results, and average wavenumbers were reported herein.

^{13}C and ^{29}Si solid state and solution NMR. Solid-state NMR spectra were collected at room temperature using an AVANCE III 200 MHz spectrometer equipped with a MAS probe. The spectra were recorded using cross polarization with high power decoupling, with samples spinning at 4.5 kHz. The number of scans was in the range of 6000–8000. The contact time and recycling delays were set at 10 ms and 2 s for ^{13}C NMR respectively. For ^{29}Si NMR, the contact time and recycling delays were set at 2 ms and 1.5 s.

For solution NMR measurements, ^{13}C and ^{1}H NMR spectra were obtained using a Bruker AV 400 MHz spectrometer. Chemical shifts are reported in ppm relative to deuterated chloroform.

Where separation was needed to isolate the cyclic carbonate prior to NMR analysis, silica gel flash chromatography was used with a 3 : 1 ethylacetate : ether mixture as solvent.

Cycloaddition reaction. Catalytic activity was evaluated using the model reaction in Scheme 7.

The reaction conditions were chosen such that the reaction was significantly away from total conversion; enabling a meaningful comparison of catalytic activity and stability. In a typical procedure, a 100 mL high pressure autoclave equipped with a magnetic stirrer was charged with 2 mL (17 mmol) of styrene epoxide (SO) and 2 mol% of organocatalyst (DMO, OMO or PMO). The reactor was directly pressurized with CO_2 to 0.5 MPa and heated to 50 °C under stirring for 5 h. At the end of the reaction, the reactor was cooled with an ice bath to ≤15 °C and CO_2 was released slowly. Then, 50 μL of dodecane (internal standard for GC analysis) was added to the reaction mixture, which was then suspended in diethyl ether and filtered off to recover the catalyst. After removal of all volatiles using a rotavap, a solvent-free reaction mixture was obtained. The spent catalyst was further stirred in acetone for 30 min, filtered off and dried in a vacuum oven at 70 °C for 2 h. TG analysis and nitrogen adsorption–desorption measurements were carried out on all spent catalysts to determine variations in N-content and textural properties.

Analysis of reaction mixture: about 0.2 μL of the solvent-free reaction mixture was injected into a Varian CP-3800 GC equipped with Agilent J&W VF-1ms capillary column (15 m length, 0.25 mm inner diameter and 0.25 μm film thickness) and a flame ionization detector (FID); with helium as carrier gas. The temperature program used for analysis was as follows: initial oven temperature 80 °C (1.5 min); ramp at 30 °C min^{-1} and held at 250 °C (3 min); injector port temperature: 200 °C; detector temperature: 250 °C. For solid reaction mixtures, 0.1 g of the mixture was dissolved in 0.2 mL of toluene, and 0.2 μL of this solution was injected into the GC.

^{13}C and ^{1}H NMR spectra of liquid samples were obtained using a Bruker AV 400 MHz spectrometer with tetramethylsilane as the internal standard. Chemical shifts are reported in ppm relative to deuterated chloroform.

Results and discussion

Characterization of mesoporous organosilicas

As shown in Fig. 1 and S1,† the nitrogen adsorption–desorption isotherms for the organosilica materials and SBA-15 were of Type IV with H1 hysteresis loop, characteristic of solids with mesopores. The corresponding textural properties and organic content are presented in Table 1. The TGA profiles of these materials may be found in Fig. 2. Compared to their pure silica, all organosilica materials derived by grafting, *i.e.* DMOs, had lower BET surface areas and pore volumes (Table 1, entries 1–8) – an indication of immobilization of organic species within the internal surface. The SBA-15 support obtained by template extraction in EtOH/HCl solution had a higher surface area and pore volume compared to that derived by calcination (Table 1, entry 7 *vs.* 9). Although thermal calcination in air can completely remove organic template, it may however cause significant framework shrinkage stemming from further silica

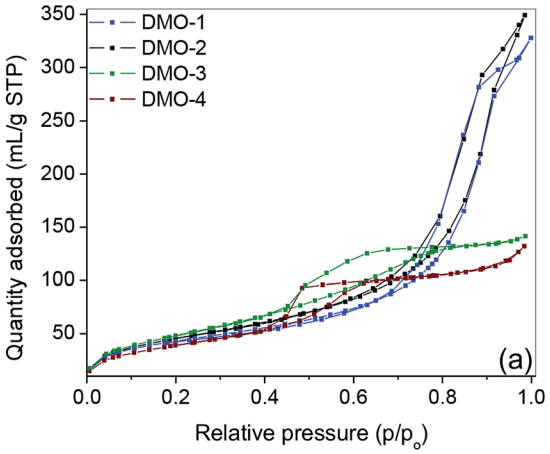

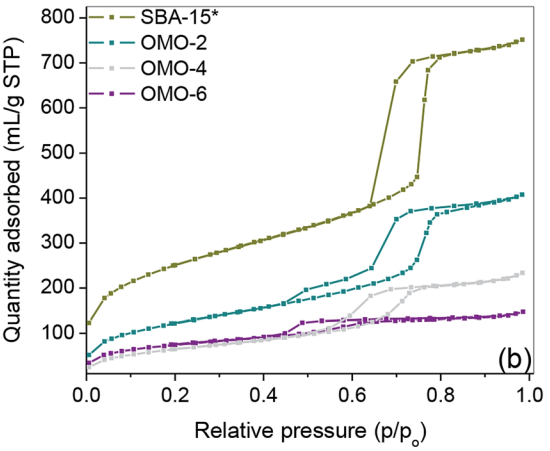

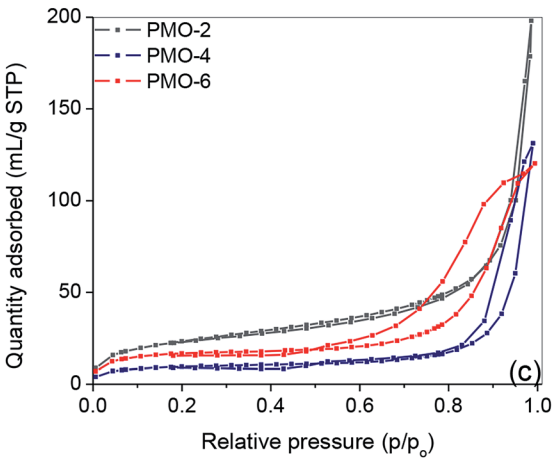

Fig. 1 Nitrogen adsorption–desorption isotherms of pristine and functionalized supports.

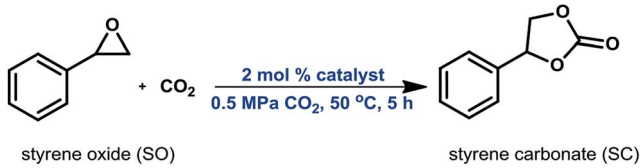

Scheme 7 Model cycloaddition reaction.

Table 1 Textural properties of solid materials

Entry	Material	Specific S.A. ($m^2\ g^{-1}$)	V_p ($mL\ g^{-1}$)	D_p (nm)	N-content ($mmol\ g^{-1}$)
1	Q-10	316	1.34	18.2	—
2	DMO-Q10	160	0.48	11.9	1.26
3	P-10	327	1.53	21.2	—
4	DMO-P10	170	0.54	12.0	1.22
5	SiL	478	0.83	9.2	—
6	DMO-SiL	182	0.22	4.6	1.37
7	SBA-15	763	1.07	7.2	—
8	DMO-SBA15	146	0.21	5.1	1.41
9	SBA-15*	913	1.23	6.18	—
10	OMO-2	449	0.66	6.0	1.22
11	OMO-4	241	0.37	5.8	1.29
12	OMO-6	270	0.22	4.1	1.22
13	PMO-2	86	0.31	15.7	2.38
14	PMO-4	34	0.20	30	2.37
15	PMO-6	60	0.18	16.7	2.11

condensation. On the other hand, template removal by solvent extraction minimizes framework shrinkage, leading to higher surface area, pore volume and number of silanols compared to its calcined counterpart.[40,41]

The capillary condensation of all DMOs and OMOs were observed to be less sharp compared to their corresponding supports and SBA-15*, respectively; an indication of decreased pore size. This provided further evidence that immobilization of the organic moieties took place on the internal surface of the supports. Compared to DMOs and OMOs, all PMOs had significantly lower surface areas, while their pore volumes were also lower than the corresponding OMOs (Table 1, entries 10 *vs.* 13, 11 *vs.* 14 and 12 *vs.* 15).

Moreover, PMOs showed a broad pore size distribution (Fig. S2†). This finding may be attributed to the higher organic content of PMOs, which adversely affects their textural properties.

Similar organic contents were measured for all amine functionalized supports and DMOs (Fig. 2a). The calculated organic content of Q-10@amine, P-10@amine, SiL@amine and SBA-15@amine were 1.59, 1.70, 1.64 and 1.80 mmol g^{-1} respectively – accounting for a grafting efficiency between 80 and 90%. This finding illustrates that despite the smaller surface areas of P-10 and Q-10 silicas compared to SiL and SBA-15, their larger pore volume and pore diameter enabled them to accommodate as much BHBPDs as SiL and SBA-15.

The N-content per gram of silica support for both S@amine solids and DMOs being the same, the yield of the quaternization reactions was evaluated to be between 92 and 97%. This finding confirms the structure of DMOs, *i.e.* as immobilized symmetrical diammonium salts. The weight lost below 200 °C of SBA-15 was <2% compared to *ca.* 10% for SBA-15* (Fig. 2b), suggesting the presence of some P123 surfactant (*vide infra*). It is known that template removal *via* solvent extraction does not completely remove the surfactant.[42] Hence, the N-content of all OMOs and PMOs were obtained taking into account the presence of about 8 wt% of surfactant. Relatively higher organic content, up to 80 wt%, was obtained for PMOs compared to DMOs and OMOs (Fig. 2c).

The ^{13}C NMR of amine@Q-10 and DMO-Q10 showed peaks around 10, 17, 51, 56, 58 and 62 ppm, which were assigned to the five carbon nuclei of BHBPD as illustrated in Fig. 3a. As-synthesized SBA-15 exhibited resonances attributed to $-CH_2-CH-$ (76 and 74 ppm) and $-CH_3$ (18 ppm) groups of the PPO, and $-CH_2-$ (71 ppm) of the PEO block of P123.[43] Following template removal by solvent extraction, ^{13}C NMR of the resultant material, SBA-15*, showed very low intensity signals between 71 and 75 ppm, and the complete disappearance of the signal at 18 ppm. Moreover, signals at 16, 50 and 59 ppm were assigned to trapped methanol and ethanol molecules used during template removal. Hence, the 8 wt% organic content of SBA-15*, as determined by TGA was assigned to the presence of small amount of template. As with DMOs, five carbon nuclei could be identified in the ^{13}C NMR of all OMOs (Fig. 3b) and PMOs (Fig. 3c).

The ^{29}Si CP MAS NMR spectra showed only Q^n species for SBA-15*, Q^n and T^n for DMOs and PMOs, and only T^n for PMOs (Fig. 3d). The characteristic resonances in the range of −89 to −118 ppm were ascribed to Q^n units, with the peaks at about −97, −102.1 and −110.9 ppm corresponding to Q^2 [$Si(HO)_2(-OSi)_2$], Q^3 [$Si(HO)(OSi)_3$] and Q^4 [$Si(OSi)_4$] species, respectively (Fig. 3d(i)). All DMOs, OMOs and PMOs showed two intense signals at *ca.* −58 and −66 ppm, attributed to Si-species covalently bonded to carbon atoms, namely T^2 [$C–Si(OH)(OSi)_2$] and T^3 [$C–Si(OSi)_3$] respectively (Fig. 3d(i)–(iv)).[44] These signals arise from immobilization of BHBPD onto the silica surface and framework of silica for DMOs and OMOs/PMOs, respectively. Furthermore, for some OMOs and PMOs, a weak shoulder at *ca.* 50 ppm, attributed to T^1 [$C–Si(OH)_2(OSi)$] species was also observed. The presence of T^1 and T^2-signals is an indication that the condensation process was not complete for these materials. Hence, the calculated nitrogen content based on TGA results, which assumes 100% condensation, may be slightly overestimated.

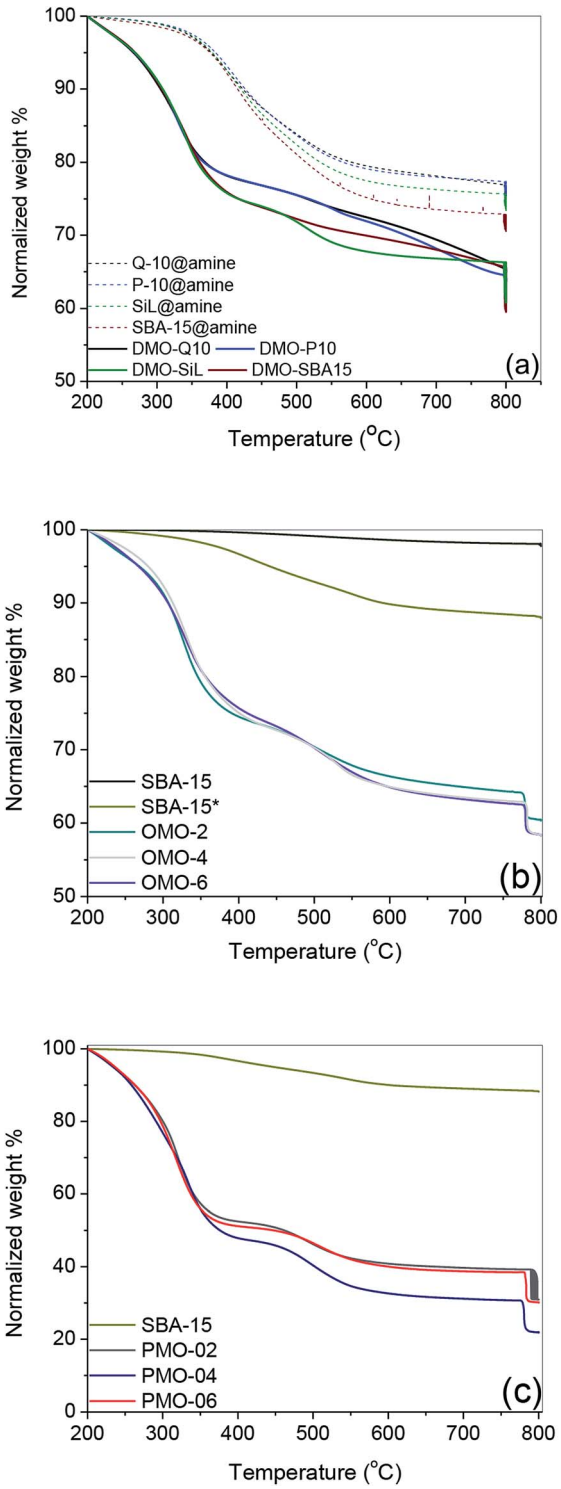

Fig. 2 TGA profile of (a) amine-functionalized supports and DMOs, (b) OMOs and (c) PMOs.

All materials showed IR absorption bands (Fig. 4 and S4†) at approximately 640, 800 and 1080 cm^{-1}, which was attributed to Si–O–Si bonds of the silicate network. The broad band centered at *ca.* 3320 or 3440 cm^{-1} were assigned to the O–H stretching vibrations of silanol groups, hydroxyl groups of BHBPD and/or adsorbed water. A band at 1650 cm^{-1} confirmed the presence of adsorbed water, whose physisorption was enhanced by the ionic nature of the –N–I bond. Furthermore, the spectra of all organosilica materials showed $–CH_2–$ stretching vibrations of the propyl chain characterized by weak absorbance at *ca.* 3030 and 2980 cm^{-1}, $–CH_2–$ bending at 1550 cm^{-1} and C–N stretching at 1450 cm^{-1}.[45] These findings are consistent with the presence of BHBPD on the silica supports. The absence of a band at 960 cm^{-1} suggests that the amount of uncondensed Si–OH groups was minimal; which is in agreement with ^{29}Si MAS NMR data. It is worth noting that bands at slightly different wavenumbers were observed for PMOs and OMOs/DMOs, suggesting differences in the chemical environment between these two groups of materials.

Catalytic activity

The catalytic activity of iodide-containing organosilicas was evaluated using the cycloaddition of CO_2 and styrene oxide (SO) to styrene carbonate (SC) under neat conditions. Because of its low activity, SO provides a more meaningful comparison than a highly active epoxide such as 1,2-epoxybutane (1,2-EB). The effect of temperature, time and CO_2 pressure on the selectivity and yield is presented in Table 2, entries 1–11. At 100 °C, 4 h and 1 MPa CO_2, yields and selectivity ≥ 97% were obtained (Table 2, entry 1) with DMO-SiL as catalysts. In an earlier study, we reported similar findings in the presence of *N*,*N*,*N*-tributyl-*N*-propylammonium iodide-functionalized mesoporous silicas.[10] These results are in agreement with other reports where immobilized ammonium[46] and phosphonium[17] salts were used. To obtain yields significantly below 100%, the following conditions were; 50 °C, 5 h and 0.5 MPa CO_2. As seen in Table 2, entries 2–11, conversion was found to be <50% for all catalysts. Amongst the DMOs, the highest yield was obtained with DMO-P10 and DMO-SiL (Table 2, entries 3 and 4). This may be attributed to smaller particle size of the silicas supports P-10 (40 μm) and SiL (40–60 μm) compared to Q-10 (75–150 μm) and SBA-15 (<150 μm).[47]

With respect to OMOs, a 45% yield of SC was obtained with OMO-2 (Table 2, entry 6). However, OMO-4 consisting of four CO_2-activating hydroxyl groups, exhibited lower activity (Table 2, entry 7), suggesting that increasing the number of hydroxyl groups from two to four was not beneficial to OMOs. A similar finding by Cheng *et al.*,[48] was attributed to an enhancement in hydrogen bond formation between the halide and additional OH groups, leading to decreased nucleophilicity or epoxide ring-opening ability of the iodide ion. Alternatively, the observed decrease in activity could originate from increase diffusion-constraints with additional ethylhydroxyl groups, such that any benefit in CO_2 activation due to extra hydroxyl groups was suppressed by slow reaction kinetics. This finding suggests that similar to homogeneous systems,[49] there is an optimal number of hydroxyl groups required for efficient activation of epoxides. A combination of diffusion-constrain and a high ratio of hydroxyl groups to organics may be at the origin of the low yield obtained with OMO-6 (Table 2, entry 8). Interestingly, OMO-4 with four hydroxyl groups, showed superior catalytic activity to all

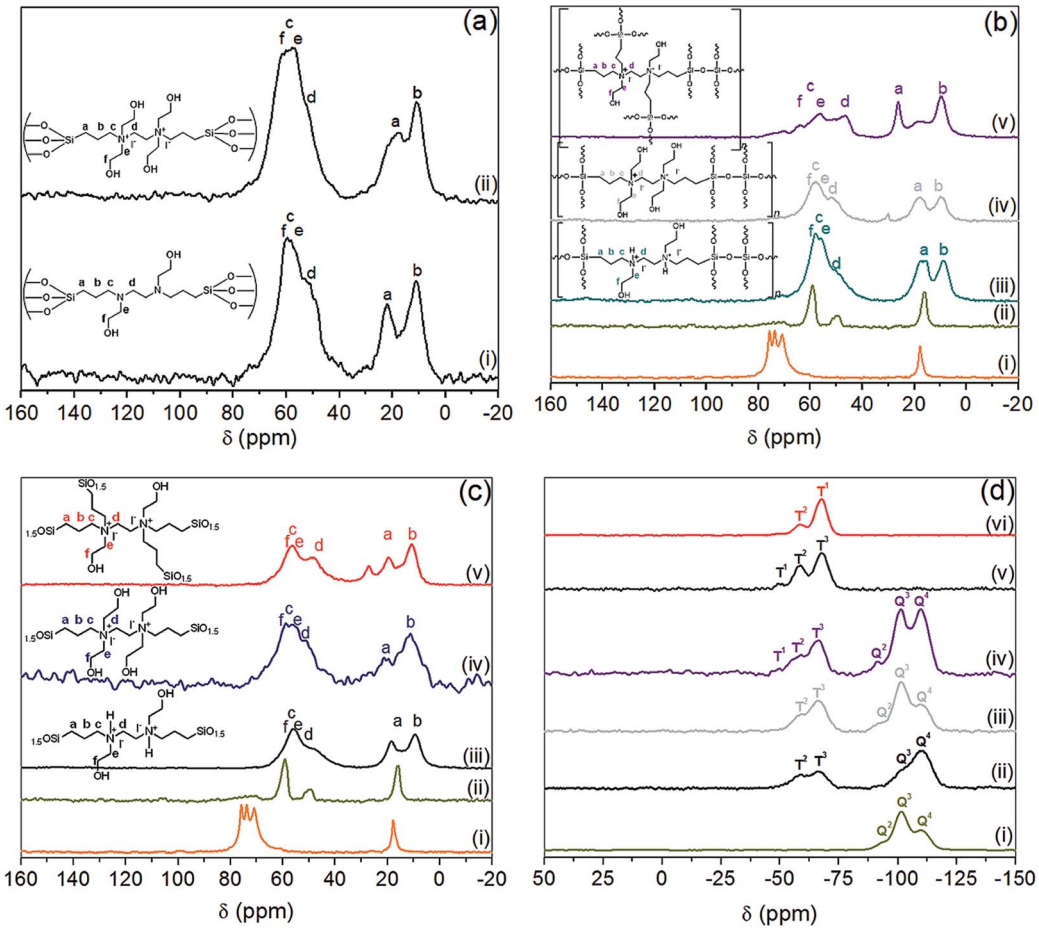

Fig. 3 ^{13}C CP-MAS NMR spectra of (a) (i) Q10@amine, (ii) DMO-Q10: (b) (i) as-synthesized SBA-15, (ii) SBA-15*, (iii) OMO-2, (iv) OMO-4, (v) OMO-6: (c) (i) as-synthesized SBA-15, (ii) SBA-15*, (iii) PMO-2, (iv) PMO-4, (v) PMO-5 and (d) ^{29}Si MAS NMR of; (i) SBA-15*, (ii) OMO-2, (iii) OMO-4, (iv) OMO-6, (v) PMO-2, (vi) PMO-6.

DMOs. This finding was attributed to the larger surface area and moderate pore volume of the latter, leading to enhanced accessibility to active sites and improved mass transport. PMOs were found to be the least active compared to DMOs and OMOs, with PMO-2 the most active of all PMOs – 24% yield (Table 2, entry 9). The inferior catalytic performance of PMOs was attributed to their low surface area, pore volume and disordered pore structure. Accordingly, OMO-2, the most active catalyst, was used to optimize the reaction conditions and material reusability.

Optimization of reaction time

Using SO as substrate, an increase in yield (44.9 to 76.9%) was observed when the reaction time was raised from 5 to 15 h (Table 2, entry 6 *vs.* 12). Compared to 1,2-EB for instance, SO is significantly more difficult to activate, and expected to take significantly longer reaction times under mild conditions to attain high yields. However, prolonged reaction times may lead to the formation of side products, ultimately reducing product yield and selectivity. Hence, optimization of reaction time was carried out with 1,2-EB. As seen in Fig. 5, the yield of 1,2-butylene carbonate (1,2-BC) was found to peak after 15 h (97.2%), which is 25% more

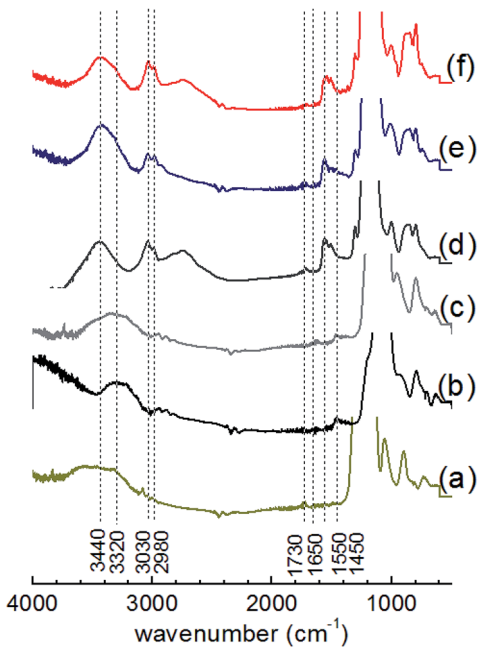

Fig. 4 IR adsorption spectra of (a) SBA-15, (b) DMO-1, (c) OMO-4, (d) PMO-2, (e) PMO-4 and (f) PMO-6.

Table 2 A comparison of the catalytic performance of different organosilica materials[a]

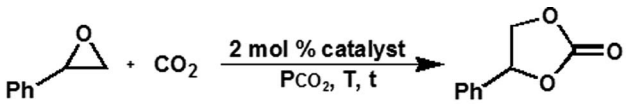

Styrene oxide Styrene carbonate

	Catalyst		Reaction condition			Reaction quantification			Spent cat.
Entry	Type	N-content (mmol g^{-1})	T (°C)	t (h)	P_{CO_2} (MPa)	Yield (%)	Sel. (%)	Yield/g cat. (%/g)	Retained N-content (%)
1	DMO-SIL	1.41	100	4	1.0	96.8	98.5	401.7	96.4
2	DMO-Q10	1.22	50	5	0.5	26.2	94.0	94.0	96.5
3	DMO-P10	1.26	50	5	0.5	31.8	98.6	117.7	93.5
4	DMO-SiL	1.41	50	5	0.5	31.6	98.5	131.1	96.8
5	DMO-SBA15	1.37	50	5	0.5	24.3	98.0	98.1	94.9
6	OMO-2	1.24	50	5	0.5	44.9	96.1	154.9	95.2
7	OMO-4	1.29	50	5	0.5	38.3	97.8	145.1	97.6
8	OMO-6	1.22	50	5	0.5	25.8	97.0	92.5	95.7
9	PMO-2	2.38	50	5	0.5	23.9	98.5	167.2	95.7
10	PMO-4	2.37	50	5	0.5	21.2	98.9	148.3	97.1
11	PMO-6	2.11	50	5	0.5	20.0	98.2	131.7	93.8
12	OMO-2	1.24	50	15	0.5	76.9	98.5	291.6	96.1

[a] Reaction conditions; 2 mol% catalysts based on N-content, 17 mmol styrene oxide (SO).

than was obtained for SC under similar conditions (Table 2, entry 12). Moreover, no noticeable change in selectivity (≥97.5%) was observed after 20 h. Nonetheless, a slight decrease in yield was recorded after 20 h, suggesting the onset of the formation of side products beyond 15 h. Hence, optimum reaction conditions for the synthesis of 1,2-BC using OMO-2 were; 2 mol% catalyst, 0.5 MPa CO_2, 50 °C and 15 h.

Reusability studies

One of the most attractive attributes of heterogeneous catalysts is their reusability. In this regard, OMO-2 was subjected to recycling experiments with 1,2-EB as substrate. As shown in Table 3, no significant changes in product yield and selectivity were observed over five cycles. Although a 7% decrease in organic content was observed compared to the fresh catalyst (Table 3, entry 1 *vs.* 2), the N-content of all spent catalyst was relatively constant, indicating the stable nature of OMO-2. This finding is consistent with the textural properties of fresh and spent catalysts being comparable.

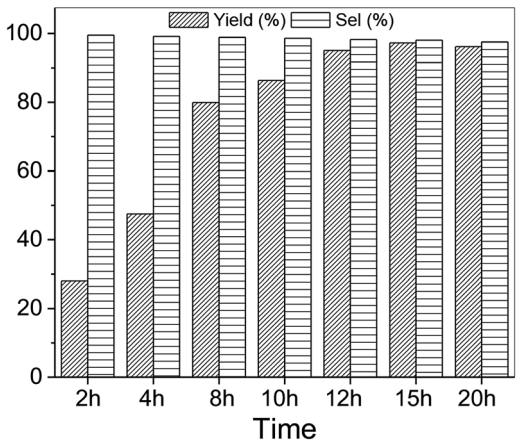

Fig. 5 Optimization of reaction time. Reaction conditions; 2 mol% catalysts, 22.7 mmol 1,2-EB.

Scope of substrates

The scope of OMO-2 was investigated using four additional substrates, namely propylene oxide (PO), epichlorohydrin (ECH), cyclohexene oxide (CHO) and 3-glycidyloxypropyltrimethoxysilane (GPS) to synthesize propylene carbonate (PC), 4-(chloromethyl)-1,3-dioxolan-2-one (4-CDO) and hexahydrobenzo[*d*][1,3]dioxol-2-one (HDO) and 4-((3-(trimethoxysilyl)propoxy)methyl)-1,3-dioxolan-2-one (4-PDO), respectively. An excellent yield (98.2%) of PC was obtained after 10 h under mild reaction conditions (Table 4, entry 1). Doubling the reaction temperature and pressure led to a very good yield (96%) after just 3 h (Table 4, entry 2). The observed marginal decreases in yield and selectively were attributed to the formation of side products, which are facilitated at higher temperatures.

Similar high yields were obtained in the synthesis of 1,2-BC and 4-(chloromethyl)-1,3-dioxolan-2-one under mild reaction conditions (Table 4, entries 3 and 5). As with the synthesis of PC, similar high yields of 1,2-BC and 4-CDO were obtained at 4 h, but at higher temperature and pressure (Table 4, entries 4 and 6). It is worth noting the high yield and selectively of these cyclic

Table 3 Reusability of OMO-2 in the synthesis of 1,2-butylene carbonate

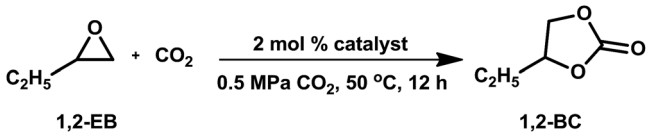

Entry	Reaction	N-content (mmol g^{-1})	Yield (%)	Sel. (%)	BET SA[a] (m^2 g^{-1})	V_p[b] (mL g^{-1})	D_p[c] (nm)
1	Run 1[d]	1.22	96.4	98.2	449	0.66	6.0
2	Run 2[e]	1.14	94.7	98.4	469	0.72	5.9
3	Run 3	1.11	95.1	98.5	453	0.68	5.9
4	Run 4	1.13	93.2	97.8	446	0.69	6.0
5	Run 5	1.12	94.3	98.0	456	0.61	6.2

[a] BET surface area. [b] Pore volume. [c] Pore diameter. [d] Fresh catalyst. [e] First reuse.

carbonates under the current mild reactions condition using a metal-free catalyst. Compared to other organocatalaysts immobilized on inert support, namely; ammonium salts on nanocrystalline zeolites,[50] imidazole-based ionic liquid (IL) on graphene oxide[51] and covalent organic frameworks,[52] triphosphonate cavitand on SBA-15,[53] phosphonium-based polymeric IL,[54] phosphonium salt on polystyrene,[55] OMO-2 was significantly more active.

As noted earlier, under the current mild reaction conditions, the yield of SC was limited to 77% (Table 4, entry 7). However, 97% yield was obtained by doubling the reaction temperature and pressure, while limiting the reaction to 4 h (Table 4, entry 8). Furthermore, reacting CHO and GPS under the current mild reaction conditions led to very low yields (Table 4, entries 9 and 11). Nonetheless, significantly higher yields were obtained at higher temperature and pressure (Table 4, entries 10 and 12). This is not surprising as these three epoxides are much more difficult to activate (due to steric hindrance) than the first three in Table 4.

Table 4 Yield and selectivity of various epoxides with CO_2 using OMO-2

Entry	Epoxide	Cyclic carbonate	P_{CO_2} (MPa)	T (°C)	t (h)	Yield (%)	Sel. (%)
1		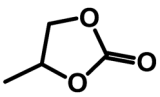	0.5	50	10	98.2	99.1
2			1.0	100	3	96.0	97.2
3	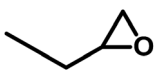	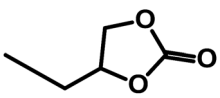	0.5	50	15	96.4	98.2
4			1.0	100	4	95.5	97.4
5	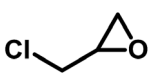	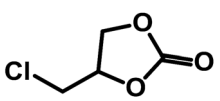	0.5	50	15	95.3	97.5
6			1.0	100	4	94.8	97.0
7	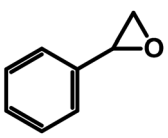	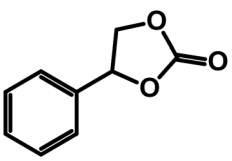	0.5	50	15	76.9	98.5
8			1.0	100	4	97.5	98.6
9	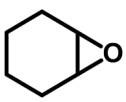	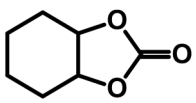	0.5	50	15	3.3	96.7
10			1.0	100	15	70.0	85.2
11	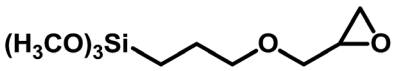	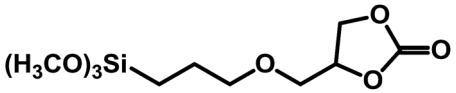	0.5	50	15	10.2	96.4
12			1.0	100	24	85.1	95.3

Conclusions

A series of novel DMOs, OMOs and PMOs were prepared, characterized and screened against the cycloaddition reaction of CO_2 and epoxides. Results showed that OMOs were the most active class of all materials. Furthermore, OMO-2, containing two hydroxyl groups per immobilized molecule was found to be the most active material. For substrates which are easy to activate such as PO, 1,2-EB and ECH, excellent yield and selectivity were obtained under mild reaction conditions (0.5 MPa CO_2, 50 °C and 10–15 h). However, higher CO_2 pressure and temperature were required with substrates which are more difficult to activate, *e.g.* SO, CHO and GPS. Furthermore, OMO-2 proved to be both chemically and structurally stable after five cycles of 1,2-EB synthesis.

Conflicts of interest

There are no conflicts to declare.

Acknowledgements

Financial support from the Natural Sciences and Engineering Research Council of Canada (NSERC) is gratefully acknowledged.

References

1 H. Ritchie and M. Roser, *Our World Data*, 2017.
2 IPCC, *Intergov. Panel Clim. Chang.*, 2018, pp. 1–32.
3 E. I. Koytsoumpa, C. Bergins and E. Kakaras, *J. Supercrit. Fluids*, 2018, **132**, 3–16.
4 J. Luis Míguez, J. Porteiro, R. Pérez-Orozco, D. Patiño and S. Rodríguez, *Appl. Energy*, 2018, **211**, 1282–1296.
5 C. Song, Q. Liu, N. Ji, S. Deng, J. Zhao, Y. Li, Y. Song and H. Li, *Renewable Sustainable Energy Rev.*, 2018, **82**(Part 1), 215–231.
6 M. Aresta, A. Dibenedetto and E. Quaranta, *J. Catal.*, 2016, **343**, 2–45.
7 M. Cokoja, M. E. Wilhelm, M. H. Anthofer, W. A. Herrmann and F. E. Kühn, *ChemSusChem*, 2015, **8**, 2436–2454.
8 J. W. Comerford, I. D. V. Ingram, M. North and X. Wu, *Green Chem.*, 2015, **17**, 1966–1987.
9 M. North, in *New and Future Developments in Catalysis - Activation of Carbon Dioxide*, Elsevier B.V., 2013, pp. 379–413.
10 J. M. Kolle and A. Sayari, *J. CO2 Util.*, 2018, **26**, 564–574.
11 H. Büttner, K. Lau, A. Spannenberg and T. Werner, *ChemCatChem*, 2015, **7**, 459–467.
12 H. Büttner, J. Steinbauer and T. Werner, *ChemSusChem*, 2015, **8**, 2655–2669.
13 L. Wang, L. Lin, G. Zhang, K. Kodama, M. Yasutake and T. Hirose, *ChemComm.*, 2014, **50**, 14813–14816.
14 X. F. Liu, Q. W. Song, S. Zhang and L. N. He, *Catal. Today*, 2016, **263**, 69–74.
15 A. Siewniak, K. Jasiak and S. Baj, *Appl. Catal. Gen.*, 2014, **482**, 266–274.
16 Y. Kumatabara, M. Okada and S. Shirakawa, *ACS Sustain. Chem. Eng.*, 2017, **5**, 7295–7301.
17 J. Steinbauer, L. Longwitz, M. Frank, J. Epping, U. Kragl and T. Werner, *Green Chem.*, 2017, **19**, 4435–4445.
18 M. North, R. Pasquale and C. Young, *Green Chem.*, 2010, **12**, 1514.
19 G. Fiorani, W. Guo and A. W. Kleij, *Green Chem.*, 2015, **17**(3), 1375–1389.
20 F. D. Bobbink and P. J. Dyson, *J. Catal.*, 2016, **343**, 52–61.
21 J. K. Lee, Y. J. Kim, Y. S. Choi, H. Lee, J. S. Lee, J. Hong, E. K. Jeong, H. S. Kim and M. Cheong, *Appl. Catal. B Environ.*, 2012, **111–112**, 621–627.
22 C. Martín, G. Fiorani and A. W. Kleij, *ACS Catal.*, 2015, **5**, 1353–1370.
23 Y. Ren, O. Jiang, H. Zeng, Q. Mao and H. Jiang, *RSC Adv.*, 2016, **6**, 3243–3249.
24 A. J. Kamphuis, F. Picchioni and P. P. Pescarmona, *Green Chem.*, 2019, **21**, 406–448.
25 T. Sakai, Y. Tsutsumi and T. Ema, *Green Chem.*, 2008, **10**, 337.
26 F. Adam, J. N. Appaturi and E. P. Ng, *J. Mol. Catal. A Chem.*, 2014, **386**, 42–48.
27 B. Chatelet, L. Joucla, J.-P. Dutasta, A. Martinez and V. Dufaud, *J. Mater. Chem. A*, 2014, **2**, 14164.
28 X. D. Lang and L. N. He, *Chem. Rec.*, 2016, 1337–1352.
29 S. Udayakumar, V. Raman, H. L. Shim and D. W. Park, *Appl. Catal. Gen.*, 2009, **368**, 97–104.
30 S. Udayakumar, S. W. Park, D. W. Park and B. S. Choi, *Catal. Commun.*, 2008, **9**, 1563–1570.
31 E. A. Prasetyanto, M. B. Ansari, B. H. Min and S. E. Park, *Catal. Today*, 2010, **158**, 252–257.
32 M. Liu, X. Lu, L. Shi, F. Wang and J. Sun, *ChemSusChem*, 2017, **10**, 1110–1119.
33 J. Peng, S. Wang, H. J. Yang, B. Ban, Z. Wei, L. Wang and B. Lei, *Fuel*, 2018, **224**, 481–488.
34 X. Zhang, W. Geng, C. Yue, W. Wu and L. Xiao, *J. Environ. Chem. Eng.*, 2016, **4**, 2565–2572.
35 J. Zhu, K. Kailasam, X. Xie, R. Schomaecker and A. Thomas, *Chem. Mater.*, 2011, **23**, 2062–2067.
36 R. Serna-guerrero, E. Da and A. Sayari, *Ind. Eng. Chem. Res.*, 2008, **47**, 9406–9412.
37 B. Lindlar, M. Lüchinger, A. Röthlisberger, M. Haouas, G. Pirngruber, A. Kogelbauer and R. Prins, *J. Mater. Chem.*, 2002, **12**, 528–533.
38 X. Feng, G. E. Fryxell, L. Q. Wang, A. Y. Kim, J. Liu and K. M. Kemner, *Science*, 1997, **276**, 923–926.
39 E. Da'na and A. Sayari, *Chem. Eng. J.*, 2011, **166**, 445–453.
40 M. Barczak, *New J. Chem.*, 2018, **42**, 4182–4191.
41 C. Knöfel, M. Lutecki, C. Martin, M. Mertens, V. Hornebecq and P. L. Llewellyn, *Microporous Mesoporous Mater.*, 2010, **128**, 26–33.
42 R. E. Mishler, A. V. Biradar, C. T. Duncan, E. A. Schiff and T. Asefa, *Chem. Commun.*, 2009, 6201–6203.
43 H. H. Oc and K. B. Yoon, *Bull. Korean Chem. Soc.*, 2008, **29**, 911–912.
44 C. Li, J. Yang, X. Shi, J. Liu and Q. Yang, *Microporous Mesoporous Mater.*, 2007, **98**, 220–226.

45 C. S. Srikanth and S. S. C. Chuang, *ChemSusChem*, 2012, **5**, 1435–1442.
46 C. Kohrt and T. Werner, *ChemSusChem*, 2015, **8**, 2031–2034.
47 M. North and P. Villuendas, *ChemCatChem*, 2012, **4**, 789–794.
48 W. Cheng, B. Xiao, J. Sun, K. Dong, P. Zhang, S. Zhang and F. T. T. Ng, *Tetrahedron Lett.*, 2015, **56**, 1416–1419.
49 J. Sun, L. Han, W. Cheng, J. Wang, X. Zhang and S. Zhang, *ChemSusChem*, 2011, **4**, 502–507.
50 B. Sarmah and R. Srivastava, *Ind. Eng. Chem. Res.*, 2017, **56**, 8202–8215.
51 J. Zhu, S. Wang, Y. Gu, B. Xue and Y. Li, *Mater. Chem. Phys.*, 2018, **208**, 68–76.
52 J. Qiu, Y. Zhao, Z. Li, H. Wang, Y. Shi and J. J. Wang, *ChemSusChem*, 2019, **12**(11), 2421–2427.
53 A. Mirabaud, A. Martinez, F. Bayard, J. P. Dutasta and V. Dufaud, *New J. Chem.*, 2018, **42**, 16863–16874.
54 Y. Liu, W. Cheng, Y. Zhang, J. Sun and S. Zhang, *Green Chem.*, 2017, **19**, 2184–2193.
55 X. Yan, R. Fu, F. Liu, Y. Pan, X. Ding and G. He, *Ind. Eng. Chem. Res.*, 2018, **57**, 3195–3203.